# A Gallery of Sky Brightness Curves from the January 2019 Total Lunar Eclipse

**Jennifer J. Birriel**
**J. Kevin Adkins**
*Department of Physics, Earth Science, and Space Systems Engineering, Morehead State University, 150 University Boulevard, Morehead, KY 40351; j.birriel@moreheadstate.edu, jkadkins@moreheadstate.edu*

**Andrea Bertolo**
*Regional Environmental Prevention and Protection Agency of Veneto, Via Ospedale Civile 24, Padova, Italy; andrea.bertolo@arpa.veneto.it*

**Rainer Ehlert**
*Citizen Scientist, Observatorio Real de 14, Cto. Real de Catorce #145, 78216 San Luis Potosí, San Luis Potosí, Mexico; rsfoto@rsfotografia.com*

**Michael McKeag**
*IDA Delegate, IDA Oregon Director, P.O. Box 130, Mosier, OR 97040; michael.mckeag@darksky.org*

**Salvador J. Ribas**
*Parc Astronomic Montsec - Ferrocarrils de la Generalitat de Catalunya, Cami del coll d'Ares s/n, E25691 Ager, Lleida, Spain; sjribas@parcastronomic.cat*

**Anthony Tekatch**
*Unihedron, 4 Lawrence Avenue, Grimsby, Ontario L3M 2L9, Canada; anthony@unihedron.com*

*Received January 19, 2020; revised March 24, April 21, 2020; accepted April 22, 2020*

**Abstract** On the night of 20–21 January 2019, a total lunar eclipse occurred for all of the Americas and most of Africa and Western Europe. We present a gallery of night sky brightness curves taken during the eclipse from eleven locations distributed through the Americas and Western Europe. Each data set was acquired using Unihedron Sky Quality Meter (SQM) pointed at zenith. In most cases, it is easy to identify the eclipse signature for the partial and total eclipse phase. The penumbral phase is undetectable due to the increasing brightness at zenith as the lunar altitude increases. A site located near the Tropic of Cancer in Mexico displays the most unusual curve: as the moon emerges from totality, the lunar altitude is very near zenith resulting in a rapid increase in brightness. These results can serve as a reference for future lunar eclipse observations using an SQM device pointed at zenith. We use the data to determine the length of the totality phase, to compare totality brightness to each site's brightness on a clear, new moon night, and finally to estimate the size of Earth's umbral shadow. Ideal observation sites would be located in the mid-latitudes of either hemisphere. We suggest future eclipse observations with SQMs be accompanied by contemporaneous all-sky imaging and data from a cloud sensor and weather station at each site to better understand the effects of lunar altitude and clouds in the field of view of each individual SQM.

## 1. Introduction

During a lunar eclipse, the full moon passes through Earth's shadow and sky brightness decreases. At totality, the brightness of the sky should theoretically approach that of a new moon night under local conditions. Published photometric studies of night sky brightness during total lunar eclipses are rare (Birriel and Adkins 2019a). We present a collection of data taken with optically identical equipment during the 20–21 January 2019 total lunar eclipse from sites across the Americas and Western Europe. We compare and contrast data sets and make suggestions for future observations.

The total lunar eclipse of January 2019 was visible in its entirety—including the penumbral, partial, and total phases—across all of the Americas and the United Kingdom (e.g. https://www.timeanddate.com/eclipse/lunar/2019-january-21). Throughout most of Europe and western Africa the total lunar eclipse phase was visible but some areas missed portions of the penumbral and/or partial phases. Across the zone of totality, the entire eclipse lasted 5 hours, 11 minutes, and 33 seconds. The totality phase of the eclipse lasted 61 minutes and 58 seconds. The geometry of the eclipse is illustrated in Figure 1.

Prior to this, there exist only two published observations of night sky brightness acquired during a total lunar eclipse. Morton recorded sky brightness during the total lunar eclipse of July 6, 1982 (Morton 1983); he used the Lowell observatory 31-inch refractor to track a patch of sky 20 degrees above the moon, tracking at lunar speed. His sky brightness curve is symmetric in the visible band, which is not surprising, given that lunar altitude relative to the patch of sky did not change. Dvorak (2005) serendipitously recorded the night sky brightness of the October 27–28, 2004, total lunar eclipse while making

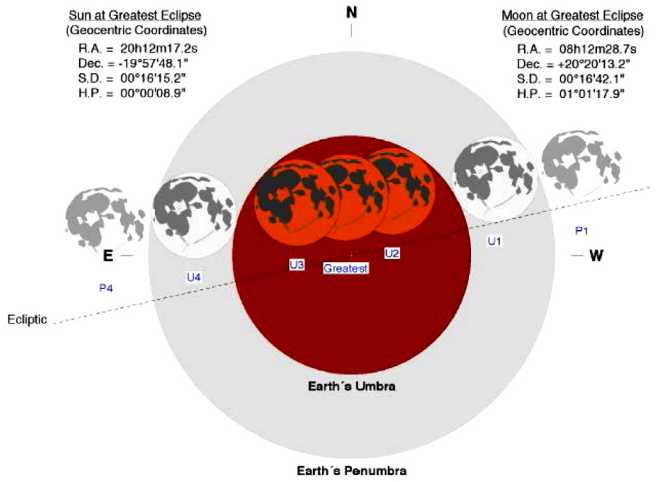


Figure 1. An illustration of the stages of the January 2019 total lunar eclipse. P1 indicates the start of the penumbral eclipse, U1 the start of the partial eclipse, and U2 the start of totality. U3 indicates the end of totality and the start of the partial eclipse. U4 signals the end of the partial phase and beginning of the penumbral phase. Finally, P4 indicates the end of the eclipse. This figure is reproduced here courtesy of Fred Espenak, www.EclipseWise.com.

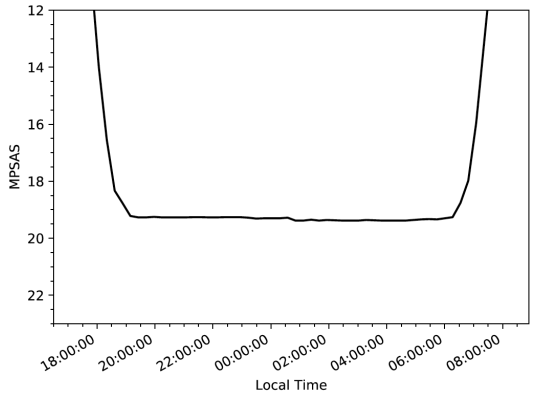


Figure 2. A clear, New Moon night at the Morehead, Kentucky observation site. These data were acquired on January 7–8, 2013, using the same SQM-LE that recorded the lunar eclipse data. These data were extracted from image plots of historical data (lost due to a hard drive failure) using the WEBPLOTDIGITIZER (Rohatgi 2019).

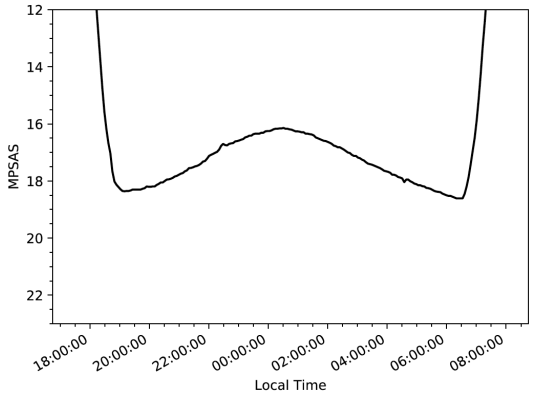


Figure 3. A clear Full Moon night at the Morehead, Kentucky observation site. These data were obtained January 26–27, 2013, using the same SQM-LE that recorded the lunar eclipse data. These data were extracted from image plots of historical data (lost due to a hard drive failure) using the WEBPLOTDIGITIZER (Rohatgi 2019).

Figure 4. An example SQM-LE installation; this is the Morehead, Kentucky site. It is located on the roof of a four-story building located away from light sources and shadowing from trees or buildings. The device is pointed at zenith.

CCD observations of the eclipsing binary QQ Cas.

Lunar eclipses occur when the moon is full. It is important to have an understanding of what sky brightness curves look like on both a full moon night and a new moon night. Figures 2 and 3 show the progression of night sky brightness at a mid-latitude location, in Morehead, Kentucky. (Recall that astronomical magnitude is an inverse scale, with lower numbers corresponding to greater brightness. Hence, we invert the y-axis in our plots so that the light curves are intuitive; a decrease on the plot corresponds to a decrease in sky brightness.) From Figure 2, a clear new moon night has a constant magnitude from the end of astronomical dusk to the start of astronomical dawn. Whereas on a full moon night, Figure 3, the night sky brightens until the moon reaches maximum altitude and then decreases as the moon's altitude decreases.

## 2. Instrumentation and observations

Unihedron Sky Quality Meters fitted with a lens (hereafter, SQM-L) are designed to perform wide-field photometric measurements of the night sky (Unihedron 2019) and have been completely characterized by Cinzano (2005, 2007). Each contains a TAOS TSL237S photodiode sensor and a HOYA CM-500 infrared blocking filter. SQM-Ls are designed to collect visible light from a cone centered at zenith. The SQM-L response to a point source, as a function of incidence angle, is bell-shaped, with a FWHM (full width at half maximum) of about 20 degrees. The response drops by a factor of 10 for a point source 19 degrees off-axis (Cinzano 2007). An onboard sensor provides temperature-corrected measurements of night sky brightness in magnitudes per square arcsecond (mpsas). Each device has a quoted uncertainty of ±0.1 mpsas.

The devices used in this study are the SQM-LU and SQM-LE. The SQM-LU is passively powered via a USB cable connected to a laptop that simultaneously controls the device

Table 1. SQM observation sites.

| *Location* | *Contributor* | *Site Description/ Conditions* | *Visible Eclipse Phases* | *SQM Interval (min)* | *Device Type* |
|---|---|---|---|---|---|
| Borrego Springs, California | M. McKeag | Rural/Partly Cloudy | P1–P4 | 0.5 | SQM-LU |
| San Luis Potosi, Mexico | R. Ehlert | Suburban/Clear | P1–P4 | 5.0 | SQM-LE |
| Morehead, Kentucky | J. J. Birriel, J. K. Adkins | Suburban/Mostly Clear | P1–P4 | 2.0 | SQM-LE |
| Grimsby, Ontario, Canada | A. Tekatch | Suburban/Overcast | P1–P4 | 5.0 | SQM-LE |
| La Silla Observatory, Chile | I. Saviane | Pristine/Clear | P1–P4 | 3.0 | SQM-LE |
| COU Station, Lleida, Spain | S. Ribas | Pristine/Fog and Stratus Clouds | P1–U4 | 0.7 | SQM-LE |
| Montseny, Barcelona, Spain | S. Ribas | Rural/Clear | P1–U4 | 0.8 | SQM-LE |
| Monte Baldo, Veneto, Italy | A. Bertolo | Rural/Fog and Partly Cloudy | P1–U4 | 5.0 | SQM-LE |
| Montebello, Veneto, Italy | A. Bertolo | Suburban/Overcast | P1–U4 | 5.0 | SQM-LE |
| Cima Ekar, Veneto, Italy | A. Bertolo | Rural/Overcast | P1–U4 | 5.0 | SQM-LE |
| Passo Valles, Veneto, Italy | A. Bertolo | Rural/Clear | P1–U4 | 5.0 | SQM-LU |

and logs data. The SQM-LE is an Ethernet-enabled version; such a device is usually installed at a permanent location and connects to a data-logging computer. An example of a permanently mounted SQM-LE is provided in Figure 4. Table 1 summarizes the locations and other relevant information of each SQM used in this study.

The data presented here are not the result of a planned, coordinated observing campaign. Retrospectively, two of the authors (Birriel and Adkins) put out a call for data from SQM sites that had collected data on the night of the eclipse. For this reason, observing intervals are not the same. However, the differences in data collection intervals do not affect the analyses that follow.

## 3. Results

Each eclipse observation, Figures 5–13, is labeled with the stages of the eclipse, denoted in Figure 1, using the known time for each phase based on the eclipse's geometry. Lunar altitudes at U1 and U4 are indicated in the upper portion of each plot. Finally, figure captions include local weather conditions retrieved from archival data available from timeanddate.com website with weather data reported in 15-minute intervals provided by CustomWeather, Inc. (2019). The analyses that follow are informed by these regional weather conditions.

Inspecting Figures 5–13, the partial and total eclipse phases are generally easy to identify. Partial phases are visible as steep changes in brightness, in the regions U1–U2 and U3–U4. Likewise, the nearly horizontal segments between U2 and U3, where the sky brightness has the largest mpsas, represents the total phase. Figure 8 is the exception; this site was experiencing overcast conditions throughout the night of the eclipse. Even in overcast conditions sky brightness decreased by approximately 1 mpsas during totality, although one might miss such a signal if they were unaware of the eclipse. On the other hand, the penumbral eclipse is not definitively identifiable in any of the observations.

## 4. Discussion

The interpretation of data such as those presented here is not trivial. We discuss the effects of cloud and lunar altitude. We also examine the scientific usefulness of sky brightness obtained during total eclipses.

### 4.1. Clouds

Clouds can affect measurements in two distinct ways. In sites free of artificial light, clouds block natural light sources in the sky, and so passing clouds will result in increased mpsas measurements (Ribas *et al.* 2016). On the other hand, at light polluted sites clouds reflect artificial light back downward; this results in decreased mpsas measurements (Kyba *et al.* 2011). Humidity has similar effects on sky brightness (Pramudya *et al.* 2019).

In addition to either increasing or decreasing sky brightness (as noted above), clouds result in "jagged" or noisy SQM data. The data from Grimsby, Ontario, Figure 8, were obtained under overcast skies; note the data are rather "noisy" with brightness variations as large as almost ± 1 mpsas. On the other hand, the larger variations in sky brightness typical of a rising moon are absent and the signature of eclipse during totality is barely visible. At Borrego Springs, California, Figure 5, conditions were partly cloudy and these data also exhibit a fair amount of noise, but the signature of the rising full moon followed by the eclipse are clearly visible. The effects of passing clouds are also evident in Figures 9, 10, and 12.

The sites in Spain and Italy are particularly interesting because they are in geographic proximity to one another. Measurements from three of these sites, Figures 10b, 11, and 13, are consistent with a decrease in sky brightness as the Moon enters Earth's penumbral shadow. However, at a nearby site in Spain, Figure 10a, we again see a large brightening. This illustrates the impact of local cloud cover on sites in geographic proximity. The stratus clouds in this pristine location did not brighten the night sky (Ribas *et al.* 2016). Here, the sky darkens due to the presence of clouds and brightens when the clouds clear, allowing moonlight through. The bright spike at U1 in Figure 10a is an example of one such clearing in the sky. We see no large spike in Figure 10b which is nearby because local cloud cover is different. The same argument would apply to Figures 12a and 12b. We suggest that the small brightening that occurs at around 1:00 am local time in Figure 13 is also due to changes in local atmospheric conditions.

### 4.2. Lunar altitude

Zenith sky brightness increases with lunar altitude, as evident in Figure 3. Although each SQM points to zenith, the angular response of the device is small, but non-negligible, at angles between 60 and 20 degrees from zenith (Cinzano 2007);

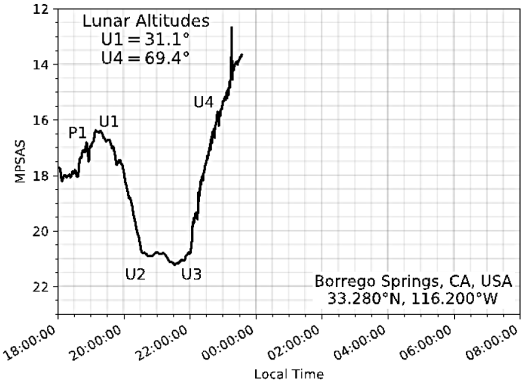


Figure 5. Borrego Springs, California: Local conditions on the night of the eclipse were partly cloudy with visibility of 10 miles and humidity averaging 80±2%. The spike just before midnight occurred when a wind gust blew the tripod over. Note here that the tail end of the first partial eclipse phase and the beginning portion of the second partial phase are difficult to distinguish from totality. The light curve is somewhat noisy and yet is quite dark: nearly 21 mpsas. Observations ended just before midnight at this site.

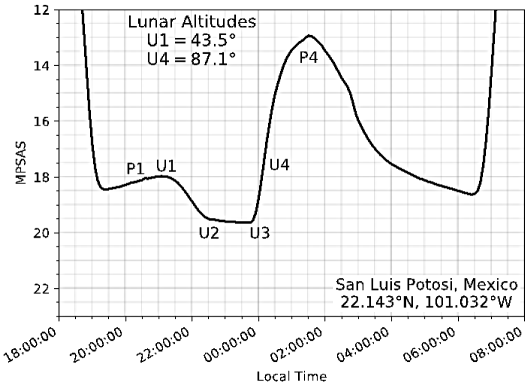


Figure 6. San Luis Potosi, Mexico: Local conditions on the night of the eclipse were clear with visibility of 10 miles and humidity averaging 70±10%. At this site, the lunar altitude is very near zenith as the partial eclipse ends, which is why the brightness increases so rapidly as the moon exits totality.

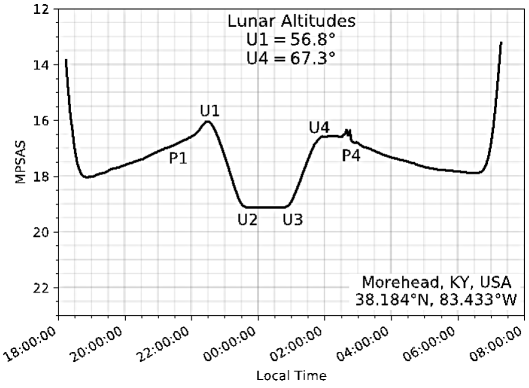


Figure 7. Morehead, Kentucky: Local conditions on the night of the eclipse were generally clear with visibility of 10 miles and humidity averaging 60±3%. According to timeanddate.com, around 9:50 p.m. there were some passing clouds, which explains the increased brightness (i.e. the bump) just as the partial eclipse begins (indicated by U1). The small feature around 2:50 a.m. is also likely due to atmospheric effects or wind.

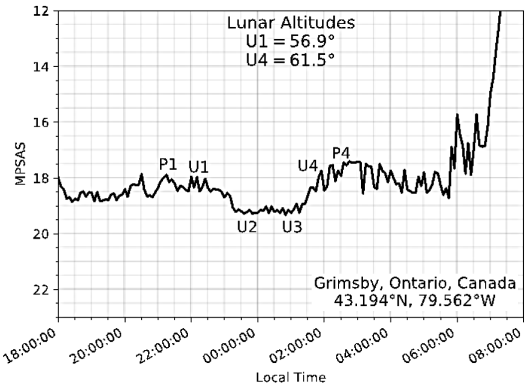


Figure 8. Grimsby, Ontario, Canada: Local conditions on the night of the eclipse were mostly cloudy to overcast with light snow, visibility of 1 mile or less, and humidity averaging 75±3%. Interestingly, here the eclipse is still seen in the sky brightness curve as a systematic decrease in sky brightness of roughly 1 mpsas.

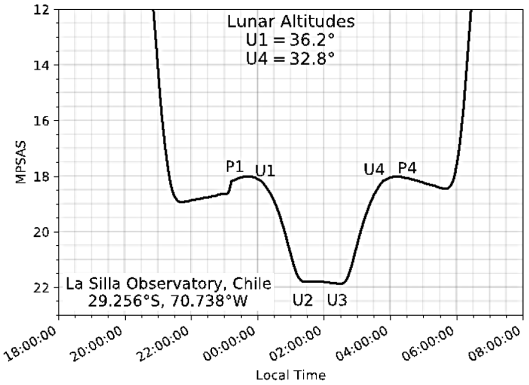


Figure 9. La Silla Observatory, Chile: Local conditions on the night of the eclipse were mainly clear with visibility of 6 miles and humidity averaging 86±5%. (These conditions are from ground stations.) The feature near 11:00 p.m. (23:00 hours) is not a discontinuity in data, but rather a smooth and sudden increase in brightness.

this effect is compounded by the fact that the sky behaves as a spherical diffuser. The effects of lunar altitude are very evident at the Mexico site, Figure 6. After totality ends and the moon moves into the penumbral shadow, there is a rapid increase in sky brightness from just over 17 mpsas to roughly 13 mpsas between the U4 and P4 stages. The lunar altitude at this site reaches 87 degrees, very near zenith. The brightness then decreases, as expected, when as the lunar altitude decreases during the second part of the night. (This same steep increase in brightness is visible in the data from California, Figure 5, where the lunar altitude is 69.4 degrees and increasing at the end of the partial eclipse phase, U4.)

During the penumbral phase of a lunar eclipse, one might expect to see a decrease in brightness, since the moon is moving into the penumbral shadow. This does appear to be the case the observation sites in Spain and Italy, see Figures 10b, 11, and 13. On the other hand, Figures 5–7, 9, and 12(a) exhibit a sky brightness that continues to increase between P1 and U1. Why might this happen? As the moon enters Earth's penumbral shadow, the moon continues to increase in altitude relative to zenith and is still a bright source, with surface brightness of approximately 4.0 mpsas when completely immersed in Earth's penumbra (Sekiguchi 1980). The effects of lunar altitude

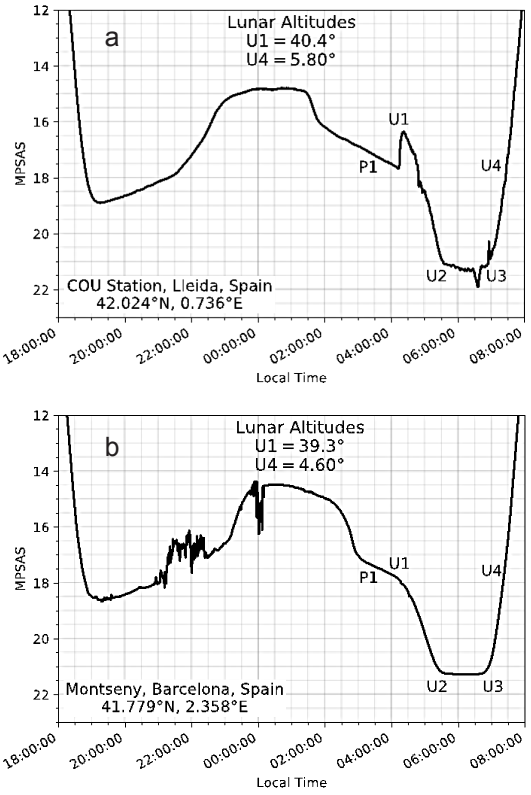


Figure 10. (a) COU Station, Lleida, Spain: Local conditions included higher humidity levels in some moments with appearance of stratus as a result of fog in the valley. (b) Montseny, Barcelona, Spain: Local conditions on the morning of the eclipse were clear and humidity averaging 80±2%. Note that at these locations, the sun begins rising as the partial eclipse is in progress.

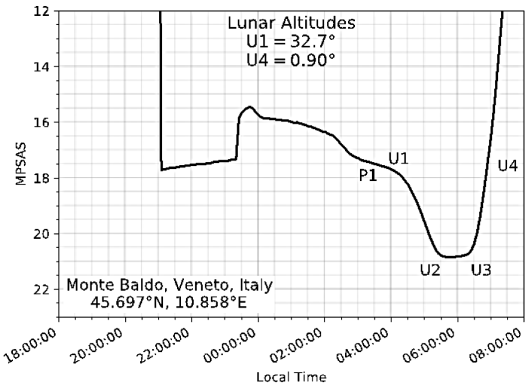


Figure 11. Monte Baldo, Vento, Italy: Local conditions on the morning of the eclipse included passing clouds and fog for ground level stations. Visibility ranged between 8 and 12 miles and humidity averaging 83±5%. At this location, the sun begins rising as the partial eclipse is in progress.

are visible in the eclipse record by Dvorak (2005), whose observations were derived from the region of sky surrounding QQ Cas and would also have been affected by changes in lunar altitude. On the other hand, Morton (1983) observed sky brightness in the region just above the moon while tracking at lunar rate and the observed sky brightness decreases smoothly as the penumbral eclipse begins.

Lunar altitude affects are likely the source of the asymmetry in the U1 and U4 phases in Figure 7. Morton (1983), whose observation technique would eliminate lunar altitude effects, reported a sky brightness curve that is symmetric on both sides

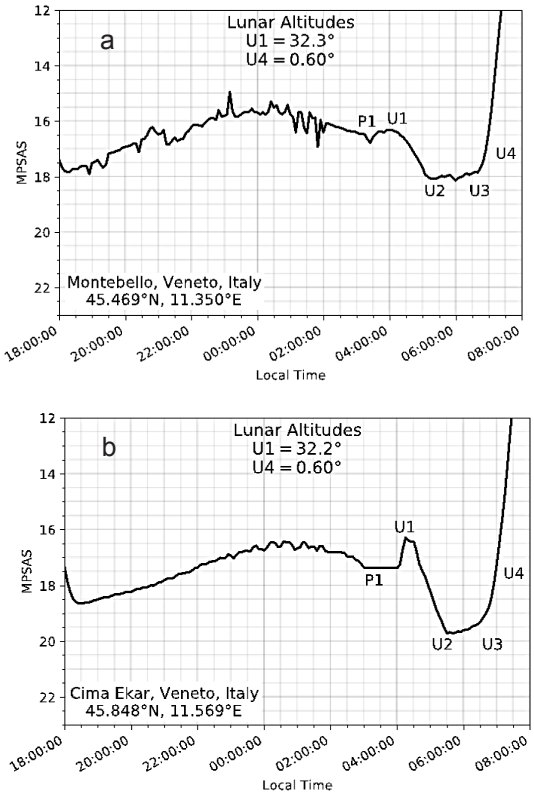


Figure 12. (a) Montebello and (b) Cima Ekar, Vento, Italy: Local conditions on the morning of the eclipse were overcast. Humidity was 81±6%. Notice that, like the Grimsby site, the eclipse is still visible despite overcast conditions but, like the other locations in Spain and Italy, the sun begins rising as the partial eclipse is in progress.

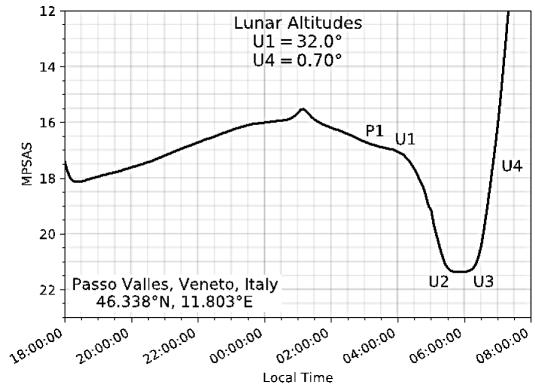


Figure 13. Passo Valles, Vento Italy: No weather data are available for this site during the hours of the eclipse. However, the hours before and after sky conditions are clear with visibility of 10 miles. The data are consistent with such conditions during the eclipse; note the smooth curve and the deep curve during partial and total eclipse phases with a totality brightness of roughly 22 mpsas. At this location, the sun begins rising as the partial eclipse is in progress.

of totality. On the other hand, Dvorak (2005), whose observation technique would have been affected by lunar altitude, also records a curve with U1 and U4 asymmetry.

### 4.3. Scientific value

We used SQM data plots to determine the duration of totality as observed at each location, see Table 2. The start and end of totality is measured on the plot by estimating where the curve is totally flat, and subsequently the associated times for U2 and

Table 2. Measured length of totality at each observation site.

| *Location* | *Length of Totality* (min)* | *Comments* |
|---|---|---|
| Borrego Springs, California | 80 ± 8 | Full eclipse visible; cloudy |
| San Luis Potosi, Mexico | 75 ± 8 | Full eclipse visible; clear; Moon at zenith at U4 |
| Morehead, Kentucky | 65 ± 8 | Full eclipse visible; mostly clear |
| Grimsby, Ontario, Canada | 95 ± 8 | Full eclipse visible; overcast |
| La Silla Observatory, Chile | 70 ± 8 | Full eclipse visible; clear |
| COU Station, Lleida, Spain | 75 ± 8 | Sun rising as total eclipse ends; fog and stratus cloud |
| Montseny, Barcelona, Spain | 65 ± 8 | Sun rising as total eclipse ends; clear |
| Monte Baldo, Veneto, Italy | 50 ± 8 | Sun rising as total eclipse ends; partly cloudy and fog |
| Montebello, Veneto, Italy | 75 ± 8 | Sun rising as total eclipse ends; overcast |
| Cima Ekar, Veneto, Italy | 60 ± 8 | Sun rising as total eclipse ends; overcast |
| Passo Valles, Veneto, Italy | 35 ± 8 | Sun rising as total eclipse ends; clear |

**Length of totality corresponds to the duration of the U2–U3 event phases.*

Table 3. Comparison of night sky brightness values between a clear, new moon night and the extracted average brightness between U2 and U3.

| *Location* | *Totality (mpsas)* | *New Moon (mpsas)* |
|---|---|---|
| San Luis Potosi, Mexico | 19.6 ± 0.1 | 19.4 ± 0.3 |
| Morehead, Kentucky | 19.1 ± 0.1 | 19.3 ± 0.3 |
| La Silla Observatory, Chile | 21.8 ± 0.1 | 22.0 ± 0.3 |
| COU Station, Lleida, Spain | 21.3 ± 0.1 | 21.7 ± 0.4 |
| Montseny, Barcelona, Spain | 21.3 ± 0.1 | 20.8 ± 0.7 |
| Monte Baldo, Veneto, Italy | 20.6 ± 0.1 | 20.6 ± 0.3 |
| Passo Valles, Veneto, Italy | 20.9 ± 0.1 | 21.3 ± 0.3 |

Table 4. Measurement of the ratio of Earth's umbral diameter to the lunar diameter.

| *Location* | *Measured Ratio* |
|---|---|
| Borrego Springs, California | 2.2 ± 0.3 |
| Morehead, Kentucky | 1.9 ± 0.3 |
| La Silla Observatory, Chile | 2.0 ± 0.2 |

U3 are read from the axis. We report a conservative 8-minute uncertainty, one quarter of the scale marking on the x-axis, for each of these measurements to allow for variation in the estimation. Interestingly, a majority of the sites do not agree with the near 62-minute time of totality. Further investigation underscores the impact that weather can have on analysis results. For easy comparison, the third column in Table 2 presents the site's weather conditions and which eclipse phases were visible. Sites with unfavorable weather, and those where the sun rises as totality ends, result in large deviations from the known time of totality. Conversely, sites with clear weather, evidenced by smooth, continuous SQM plots, agree well with the known time of totality.

The depth of the eclipse in terms of SQM readings depends on lunar distance (which is the same for all sites) and local sky conditions including lunar altitude and local light pollution and is not particularly valuable. On the other hand, the SQM reading during totality should be similar to the sky brightness on a clear, new moon night; where possible we have made appropriate comparisons using an average value extracted between U2 and U3 from the data, see Table 3. Because clouds are known to increase sky brightness at light polluted sites, sites with clouds are excluded from the comparison. For the remaining sites, we find excellent agreement between totality and a new moon. For the uncertainties for the new moon night we assume a canonical value of ± 0.3 mpsas typically of seasonal variations (e.g. Plauchu-Frayn *et al.* 2017; Posch, Binder, and Puschnig 2018). The sites in Spain have long-term observations and we quote the known variations in season for these. Since totality measurements represent a single measurement these are subject only to the known SQM uncertainty of ± 0.1 mpsas (Cinzano 2007).

Birriel and Adkins (2019b) suggest a method to estimate the size of Earth's umbral shadow using sky brightness curves. We employ their method and present results in Table 4 for sites where the U1 through U4 phases are clearly identifiable. On average, Earth's umbral shadow has a diameter of 2.65 lunar diameters for central eclipses, those where the moon passes through the center of Earth's shadow. We find that the ratio of Earth's umbral diameter to the lunar diameter is in agreement between all sites. However, the values are collectively smaller than the known umbral diameter; this result is not unexpected since this eclipse is a non-central one (Birriel and Adkins 2019b).

What makes the most scientifically useful data set? Ideal sites are those with generally clear sky conditions and from which all phases of the eclipse, P1–P4, can be clearly identified. Mid-latitude sites are ideal while sites between the Tropics of Cancer and Capricorn would not provide much useful data. It is important that each site have contemporaneous sky and weather conditions available for interpretation of unusual features. (For example, Figure 9 exhibits a sudden brightening at around 11:00 p.m. local time, around the time the partial eclipse begins. It appears to be a discontinuity in data, but it is not. The sky was clear at this site and the lunar altitude was approximately 30.2 degrees which is just at the limit of the SQM's angular sensitivity. Is this effect the result of instrument sensitivity or changes in humidity or other atmospheric conditions? Without a detailed record of local sky conditions, we cannot say with certainty.) While archival weather data are useful, they are generally regional in nature. The ideal instrumental suite to accompany an SQM site would include an all-sky camera to monitor both clouds and the moon, a cloud sensor, and a weather

station (or data from the closest possible weather station, such as an airport).

## 5. Conclusions

We have presented measurements of night sky brightness during the January 20–21, 2019, total lunar eclipse as recorded by SQM-L devices at 11 different locations across the Americas and Western Europe. The data show the signature of the eclipse is generally quite distinct for the partial and total phases. On the other hand, the signature of the penumbral phase is more difficult to discern due to the combination of lunar altitude and the device's angular response at angles off zenith. Meaningful comparisons of data from different sites require detailed information regarding cloud cover, humidity, and lunar altitude. Interpretation of such light curves is paramount if one wishes to use these to extract information regarding eclipse phases and their duration. For example, estimating the size of Earth's umbral shadow requires identification of the U1 through U4 phases of the eclipse in a sky brightness curve recorded during a total eclipse.

Given the proliferation of SQM devices for light pollution research, this gallery should prove useful for future eclipse observations, and the authors propose coordinated observing campaigns for future lunar eclipses. Ideal observation sites would be located in the mid-latitudes of either hemisphere, where the lunar altitude does not exceed 70 degrees during the eclipse. Future SQM observers should collect data from the same site on both clear new moon nights and clear full moon nights, ensuring a baseline for comparison to the eclipse data. Those with access to a self-contained, autonomous SQM-LU-DL should select a dark sky site with high probability of a clear sky. It is also important that observers accurately synchronize all clocks (laptop, SQM, cameras, weather stations, and cloud sensors).

## 6. Acknowledgements

The authors wish to thank the La Silla Observatory Site Manager, Dr. Ivo Saviane, for his data contribution to this study. Additionally, we want to acknowledge that all of the data plots presented in this paper were created with the Matplotlib library in PYTHON (Hunter 2007). We thank Fred Espenak (www.EclipseWise.com) for allowing us to reproduce the geometry of the January 2019 eclipse (Figure 3). The authors also wish to thank the anonymous referee whose comments and suggestions improved both the readability and quality of this paper.

## References

Birriel, J., and Adkins, J. K. 2019a, *J. Amer. Assoc. Var. Star Obs.*, **47**, 94.

Birriel, J., and Adkins, J. K. 2019b, *Amer. J. Phys.*, **87**, 994.

Cinzano, P. 2005, *ISTIL Internal Rep. No. 9*, v.1.4, 1.

Cinzano, P. 2007, *ISTIL Internal Rep. No. —*, v.0.9, 1.

CustomWeather, Inc. 2019, weather information (https://customweather.com/ (via https://www.timeanddate.com/weather)), accessed 12 December 2019.

Dvorak, S. 2005, *J. Amer. Assoc. Var. Star Obs.*, **34**, 72.

Hunter, J. D. 2007, *Comput. Sci. Eng.*, **9**, 90.

Kyba, C. C. M., Ruhtz, T., Fischer, J., and Hölker, F. 2011, PLoS One, 6, e17307 (https://journals.plos.org/plosone/article?id=10.1371/journal.pone.0017307).

Morton, J. C. 1983, *Obs.*, **103**, 24.

Plauchu-Frayn, I., Richer, M. G., Colorado, E., Herrera, J., Córdova, A., Ceseña, U., and Ávila, F. 2017, *Publ. Astron. Soc. Pacific*, **129**, 035003.

Posch, T., Binder, F., and Puschnig, J. 2018, *J. Quant. Spectrosc. Radiat. Transfer*, **216**, 56.

Pramudya, Y., Budi, K. S., Okimustava, and Muchlas. 2019, in *Journal of Physics Conference Series 1231*, issue 1, article id. 012004.

Ribas, S. J., Torra, J., Figueras, F., Paricio, S., and Canal-Domingo, R. 2016, *Int. J. Sustainable Lighting*, 18, 32.

Rohatgi, A. 2019, WEBPLOTDIGITIZER (https://apps.automeris.io/wpd).

Sekiguchi, N. 1980, *Moon and Planets*, **23**, 99.

Unihedron. 2019, Unihedron Sky Quality Meter (http://unihedron.com/projects/sqm-le/), accessed 28 December 2019.